Key Determinants of Selective Binding and Activation by the Monocyte Chemoattractant Proteins at the Chemokine Receptor CCR2

Zil e Huma[1], Julie Sanchez[1], Herman D. Lim[2], Jessica L. Bridgford[1,2], Cheng Huang[1], Bradyn J. Parker[1], Jiann G. Pazhamalil[1], Benjamin T. Porebski[1], Kevin D. G. Pfleger[3], J. Robert Lane[2], Meritxell Canals[2,*] and Martin J. Stone[1,*]

Affiliations:

[1] Infection and Immunity Program, Monash Biomedicine Discovery Institute, and Department of Biochemistry and Molecular Biology, Monash University, Clayton, VIC 3800, Australia.

[2] Drug Discovery Biology, Monash Institute of Pharmaceutical Sciences, Monash University, Parkville, VIC 3052, Australia.

[3] Molecular Endocrinology and Pharmacology, Harry Perkins Institute of Medical Research, QEII Medical Centre, Nedlands; Centre for Medical Research, The University of Western Australia, Crawley and Dimerix Bioscience Limited, Nedlands, Western Australia, Australia.

*To whom correspondence should be addressed: martin.stone@monash.edu or meri.canals@monash.edu

Abstract

Chemokines and their receptors collectively orchestrate the trafficking of leukocytes in normal immune function and inflammatory diseases. Different chemokines can induce distinct responses at the same receptor. In comparison to monocyte chemoattractant protein-1 (MCP-1/CCL2), the chemokines MCP-2/CCL8 and MCP-3/CCL7 are partial agonists of their shared receptor CCR2, a key regulator of monocyte/macrophage trafficking. Using chimeras of MCP-1 and MCP-3, we have identified the chemokine N-terminal region as being the primary determinant of the binding and signaling selectivity of these two chemokines at CCR2. Analysis of CCR2 mutants showed that the chemokine N-terminus interacts with the major subpocket in the transmembrane helical bundle of CCR2 as distinct from the interactions of some other chemokines with the minor subpockets of their receptors. These results suggest the major subpocket as an excellent target for development of CCR2 small molecule inhibitors.

One Sentence Summary: Interactions of different chemokine N-termini with the transmembrane bundle of a shared receptor induce distinct signaling responses.

Introduction

G protein-coupled receptors (GPCRs) are the largest family of transmembrane receptors and the targets of numerous therapeutics. Many GPCRs can be activated by a variety of different natural and/or synthetic agonists, which may give rise to distinct signaling outcomes. Whereas partial agonists evoke a submaximal response relative that of a full agonist even at concentrations that saturate all receptor sites, biased agonists can display pathway-dependent efficacy, activating certain pathways to the relative exclusion of others (*1, 2*).

The recent flood of GPCR structures has yielded a wealth of new information regarding receptor architecture, ligand binding sites and G protein binding sites as well as some details of the conformational changes associated with receptor activation (*3-5*). Consequently, we can now begin to identify the structural mechanisms by which different agonists induce distinct signaling outcomes. Herein we describe an analysis of the structural features underlying differential activation of a chemokine receptor by its cognate chemokine ligands.

Chemokine receptors are GPCRs expressed in leukocyte membranes, whereas chemokines are small, soluble proteins expressed in tissues during normal immune surveillance or in response to injury or infection. Activation of chemokine receptors by their cognate chemokines induces leukocyte migration into, and accumulation in, the chemokine-expressing tissues (*6-8*), a hallmark feature of the inflammatory response. Consequently, chemokine receptors are potential therapeutic targets in a wide range of inflammatory diseases (*9*). There is increasing evidence that cognate chemokines can differentially activate their shared receptors, including examples of partial agonism (*10-14*) and biased agonism (*15, 16*).

CCR2 is the major chemokine receptor on monocytes and macrophages, cells that play central roles in the pathology of atherosclerosis, obesity and type 2 diabetes. In atherosclerosis, CCR2 activation by the monocyte chemoattractant proteins MCP-1 (systematic name CCL2), MCP-2 (CCL8)

and MCP-3 (CCL7) induces recruitment of monocytes from the blood into arterial walls, where they differentiate into macrophages and contribute to development of atherosclerotic plaques (*17*). In obesity, CCR2 activation by MCP chemokines is associated with macrophage infiltration into adipose tissue and induction of insulin resistance (*18*). Considering the importance of CCR2 in inflammatory diseases, there is strong motivation to understand its mechanism of activation by its cognate chemokine ligands.

Although their distinct biological functions are not fully understood, the MCP chemokines are differentially expressed in response to Th1 versus Th2 inflammatory stimuli and can have distinct temporal patterns of expression, suggesting that they may also activate distinct cellular responses via their shared receptor (*19, 20*). In support of this possibility, Berchiche *et al*. have shown that cognate chemokines for CCR2 display differences in their efficacies of activation of both β-arrestin and G protein-mediated signaling pathways (*13*). Here, we verify that this differential signaling can be attributed to partial agonism rather than biased agonism and we use a variety of chemokine chimeras and CCR2 mutants to identify key structural elements of both the chemokines and receptor that mediate this differential activation. Data are interpreted in light of the recent structures of chemokine-receptor complexes (*21, 22*), yielding insights towards the design of selective pharmacological agents.

Results

MCP chemokines have different efficacies and affinities at CCR2

We monitored activation of CCR2 by MCP chemokines using one proximal, non-amplified measure of receptor activation (recruitment of β-arrestin 2) and two downstream, amplified signals (inhibition of cAMP formation and phosphorylation of ERK1/2). The three chemokines induced recruitment of β-arrestin 2 (β-arr2) with different potencies and significantly different maximal

effects, E_{max} (Fig. 1A, Table 1); relative to MCP-1, the E_{max} of MCP-2 and MCP-3 were 23 ± 3% and 56 ± 4%, respectively. In the two amplified signaling assays, the three chemokines exhibited the same maximal effect as each other but significantly different potencies, and higher potencies than in the β-arr2 assay (Fig. 1, B and C; Table 1). The order of potencies between the three agonists in the amplified assays was the same as the order of their maximal effects in the proximal assay. Moreover, the same rank order of binding affinities was also observed in a radioligand binding assay (Fig. 1D; Table 1). These results are in good agreement with the effects of MCP chemokines reported previously (*13*).

Analysis of our data using an approach based upon the operational model of agonism (*23, 24*) indicated that the MCP chemokines did not display biased agonism (fig. S1; Table S1) but instead that MCP-2 and MCP-3 are partial agonists of CCR2, relative to MCP-1. The data in Fig. 1, A to D highlight two underlying differences in the receptor interactions of the MCP chemokines. First, the three chemokines have different affinities for CCR2 (Fig. 1D). Second, the three chemokines have different maximal effects in the proximal β-arr2 recruitment assay (Fig. 1A). Although the rank order of these maximal effects is the same as the rank order of affinities for the three chemokines, the maximal effects occur at ligand concentrations at which the receptor is fully occupied so they do not result from differences in binding affinity. Instead, they indicate that the ligands have distinct efficacies, i.e. distinct intrinsic abilities to induce the receptor-mediated response.

In the more amplified assays (inhibition of cAMP and ERK1/2 phosphorylation), the maximal effects of full and partial agonists are indistinguishable (the signals are amplified to the full capacity of the pathway even when the activated state of the receptor is only partially populated). In such assays the relative potency of the chemokines is determined by both the affinities of the chemokines for CCR2 and their relative efficacies (*25*). Indeed, the order of potency in the cAMP

and pERK assays is consistent with both their relative affinities for the receptor and their relative E_{max} values in the proximal assay (Fig. 1, A to D).

An important consequence of partial agonism in the context of the β-arrestin assay is that subsequent regulatory processes, such as receptor internalization, will also be submaximally engaged by the action of partial agonists. In agreement with the work of Berchiche et al. (*13*), both MCP-2 and MCP-3, at saturating concentrations, caused very limited internalization of CCR2, whereas MCP-1 induced significant internalization (Fig. 1E). These differences correlate with the relative efficacies of the three chemokines.

Considering the robust and consistent differences observed among the MCP chemokines for CCR2 binding and activation (Fig. 1), this system is ideally suited for investigation of the structural features influencing the relative affinities and efficacies of different chemokines at their shared receptor, as described below.

The chemokine N-terminal tail is a major determinant of affinity and efficacy

Mutational and structural studies have previously identified three regions of chemokines that interact with receptors (*26-29*). The so-called "N-loop" (a ~12 residue sequence between the conserved CC or CXC motif and the first β-strand) and the β3 region (third β-strand and preceding turn) form the two sides of a shallow groove that binds to the flexible N-terminal tail of the receptor. The N-terminal region of the chemokine (preceding the CC or CXC motif) penetrates into the transmembrane helical bundle of the receptor. To identify the structural elements of MCP chemokines that contribute to partial versus full agonism and to relative CCR2 affinity, we prepared a series of chimeras in which these three functionally important regions are swapped between MCP-1 and MCP-3 (Fig. 2); MCP-3, rather than MCP-2, was chosen primarily because it is more closely related to MCP-1, thereby simplifying the interpretation of chimera experiments (see

Supplementary Material). Each chimera is named according to the parental chemokine from which it is derived followed by a sequence of three numbers representing the origin of the N-terminal, N-loop and β3 elements, respectively; for example, MCP1-133 is a chimera derived from MCP-1 and containing the N-terminal region of MCP-1, the N-loop of MCP-3 and the β3 region of MCP-3. Each chimera was expressed as inclusion bodies in *E. coli*, refolded and purified. ^{1}H NMR spectra (Fig. 2 and fig. S2) are similar to those of the wild type (WT) chemokines, indicating that the chimeras are well folded and adopt the expected native 3D structures.

To assess the contributions of the three chemokine structural regions to CCR2 binding affinity, we measured the abilities of the MCP chimeras to compete with ^{125}I-MCP-1 binding to CCR2. As shown in Fig. 3, A and E, and Table 2, MCP-1 has 10-fold higher affinity than MCP-3 at CCR2. Replacement of the N-terminus of MCP-1 with that of MCP-3 caused a decrease in affinity such that this chimeric chemokine displayed an affinity comparable to that of MCP-3. Similarly, replacement of the N-terminus of MCP-3 with that of MCP-1 generated a chimeric chemokine with comparable affinity to that of MCP-1. These results clearly indicate that the N-terminus of MCP-1 has a significant role in determining its higher affinity as compared to MCP-3.

In contrast to the clear contribution of the N-terminal region to binding selectivity, replacement of the N-loop and/or β3 region of MCP-1 with that of MCP-3 did not affect the CCR2 binding affinity. Similarly, substitution of the β3 region of MCP-3 with that of MCP-1 had no significant effect on affinity. However, replacement of the N-loop of MCP-3 by that of MCP-1, alone or in combination with the β3 region (chimeras MCP3-313 and MCP3-311) reduced the affinity for CCR2. This is consistent with the previous findings that the N-loop is a major contributor to CCR2 binding but also suggests that the ability of the N-loop to interact favorably with the receptor is dependent on the background scaffold in which it is located. Notably, subsequent introduction of the MCP-1 N-terminal region, to give the MCP3-111 chimera, increased CCR2 affinity 100-fold

(relative to MCP3-311), again highlighting the importance of the N-terminus as a determinant of chemokine affinity at CCR2.

To assess the contributions of the three chemokine structural regions to the efficacy of CCR2 activation, we measured the abilities of the chemokine chimeras to stimulate β-arr2 recruitment (Fig. 3B). As described above, MCP-3 displayed a significantly lower maximal effect than MCP-1 (Fig. 1A; Fig. 3, B and E). Replacement of the N-loop and/or the β3 region of MCP-1 with those of MCP-3 (or *vice versa*) caused no significant changes in E_{max}. In contrast, replacement of the N-terminus of MCP-1 with that of MCP-3, alone or in combination with replacement of both the N-loop and β3 region, caused a significant decrease in maximal effect compared to MCP-1, to a level comparable to the maximal effect of MCP-3. This vital role of the N-terminus in determining chemokine efficacy at CCR2 was further highlighted in the reciprocal chimeras whereby integration of the N-terminus of MCP-1 into an MCP-3 background (MCP3-133 and MCP3-111) resulted in a significant increase in the maximal effect. Interestingly, the E_{max} values of these two chimeras were greater than that of wild type MCP-1, again emphasizing that the background chemokine "context" plays an additional role in determining efficacy at CCR2.

In addition to the above E_{max} values, our data also report on the potencies of the chemokine chimeras in the β-arr2 recruitment. Although, we observed no significant differences in the potencies (Fig. 3E; Table 2), the order of potencies is consistent with the order of binding affinities and of E_{max} values described above. Similarly, at a more amplified signaling endpoint of ERK1/2 phosphorylation (Fig. 3, C and E), replacing the N-terminus of MCP-1 by that of MCP-3 caused a decrease in potency whereas replacing the N-terminus of MCP-3 by that of MCP-1 caused an increase in potency, although these effects did not reach significance (Fig. 3E; Table 2).

In the ERK1/2 phosphorylation assay, the two wild type chemokines and most chimeras displayed similar maximal effects (Fig. 3E; Table 2), However, chimera MCP3-111 displayed a

significantly lower E_{max} than wild type MCP-3 in the ERK1/2 phosphorylation assay despite exhibiting a significantly higher E_{max} than MCP-3 in the β-arr2 assay. Further analysis (fig. S3 and Table S3) indicated that this chimera displayed significant biased agonism relative to WT MCP-3, suggesting that the three substituted regions of the chemokines may act cooperatively to influence signaling efficacy in a pathway specific manner.

From these data it is clear that the N-termini of MCP-1 and MCP-3 have important roles in determining the relative affinities of the different chemokines at CCR2 as well as their relative efficacies. Based on these results, we predicted that the chimeric chemokines in which the N-terminal regions were swapped would have altered abilities to induce CCR2 internalization. As expected, MCP1-311 lost its ability to internalize the CCR2, while the reciprocal N-terminal swap chimera (MCP3-133) was now able to induce receptor internalization (Fig. 3D).

Identification of CCR2 residues contributing to differential chemokine binding and agonism

In light of the above observations that the chemokine N-terminal regions contribute to both the affinity of CCR2 binding and the efficacy of CCR2 activation, we sought to identify the residues within CCR2 with which the chemokine N-terminal regions interact. Recent structures of two chemokine-receptor complexes (*21, 22*) have confirmed that the N-terminal regions of chemokines penetrate into the transmembrane (TM) helical bundles of their receptors, where they presumably induce structural rearrangement and signaling. To identify specific residues of CCR2 that contribute to these interactions, we characterized chemokine binding and activation for a series of CCR2 mutants. Guided by a homology model of the MCP-1:CCR2 complex, which was based on the reported structure of receptor CXCR4 cross-linked to chemokine vMIP-II (*21*), we designed six point mutants and four double mutants at positions pointing towards the interior of the TM bundle (Fig. S4; Table 3). Each mutant was stably expressed in FlpIn HEK-293 cells with an N-terminal cMyc

epitope tag, enabling measurement of cell surface expression. After confirming that all mutants were expressed at similar levels to WT CCR2 (Table 3), we evaluated the affinity of chemokine binding at each mutant receptor. We extended this evaluation to measure the potency and efficacy of MCP-1 and MCP-3 at the mutant receptors using ERK1/2 phosphorylation as a convenient measurement of receptor activation that does not require the use of modified receptor fusion constructs or overexpression of signaling effectors.

None of the mutations significantly changed the affinities for MCP-1 or MCP-3 compared to WT CCR2 (Table 3; Fig. 4A; fig. S5). However, comparison of the relative affinities of MCP-1 and MCP-3 at the different mutants was more revealing. MCP-3 displays a 10-fold lower affinity than MCP-1 at the WT CCR2. While this difference in affinity was maintained at the majority of the CCR2 mutants, no such difference in affinity was observed at the R206A and Y259F mutations. Therefore, the difference in affinity between MCP-1 and MCP-3 appears to be governed, at least in part, by these two residues.

As shown previously at WT CCR2, MCP-1 displays a significantly higher potency than MCP-3. This difference in potency was maintained across most mutants, in accordance with the relative affinities for the two ligands (Fig. 4B; fig. S5). Nevertheless, mutant Y259F displayed increased potency for both chemokines; double mutant I263A/N266A displayed significantly increased potency for MCP-1 ($p = 0.003$) and a smaller, but not significant, increase for MCP-3; and D284A showed a significant potency increase for MCP-1 but not MCP-3 (Fig. 4B).

Although the potencies of ERK1/2 phosphorylation correlate well with CCR2 binding affinities for the wild type chemokines (Fig. 1), there is a poor correlation between affinity and potency comparing the same chemokine across the set of CCR2 mutants (fig. S6, A and B). This suggests that some of the mutations influence the mechanism of receptor signaling rather than ligand binding. To further explore this possibility, we examined the maximal effects induced by the two chemokines in

the ERK1/2 phosphorylation assay (Fig. 4C; fig. S5; fig. S6C). CCR2 mutants Y120F, R206A, E270A/F272A and E291A displayed significantly lower E_{max} values for both MCP-1 and MCP-3 as compared to WT CCR2. Interestingly, the maximal effect of MCP-1 but not MCP-3 was significantly reduced at the I263A/N266A mutant. Conversely, the double mutant N199A/T203A displayed a significantly reduced E_{max} for MCP-3 but not MCP-1. Finally, the mutation K34A caused an increase in E_{max} relative to WT for MCP-1 and a similar trend was observed for MCP-3. It should be noted that the cell surface expression levels for all mutants was not significantly different. Thus, these changes in maximal signaling likely reflect the roles of these residues in conformational rearrangement of CCR2 coupled to ERK1/2 signaling pathways.

Discussion

Humans and other mammals express a complex array of chemokines and receptors that collectively orchestrate the trafficking of leukocytes, a central feature of the innate immune response. The existence of multiple chemokines that activate the same receptor was previously thought to represent functional redundancy. However, recent results, including observations of partial agonism (*10-14*) and biased agonism (*15, 16*) increasingly suggest that different chemokines are able to alter receptor responses in a subtle and selective manner. In this study, we have begun to elucidate the structural features underlying the partial agonism of MCP chemokines at their shared receptor CCR2.

Numerous previous structure-function studies of chemokines have identified residues within the N-loop and β3 region as being critical for binding interactions and residues within the N-terminal region as being critical for receptor activation (*26-29*). These conclusions are encapsulated by the two-site model, which postulates that chemokines first use their N-loop/β3 residues (chemokine site 1; CS1) to bind to the receptor N-terminus (receptor site 1; RS1) and subsequently the

chemokine N-terminus (chemokine site 2; CS2) activates the receptor by binding to its transmembrane helices (receptor site 2; RS2), inducing conformational changes and cellular signaling (*29*). The presumption that binding and activation occur in two discrete steps rather than concomitantly is not derived from kinetic measurements but instead deduced from indirect evidence such as the ability of N-terminally truncated chemokines to bind strongly without activating their receptors (*30, 31*). Recent structures of two chemokine-receptor complexes (*21, 22*) helped to validate key features of the two-site model but also suggested that the two sites may not be completely independent. As discussed in a recent, comprehensive review (*32*), a number of additional observations have also suggested that elaborations of the two-site model may be necessary. In summary, although the two-site model is broadly supported by structural and mutational data and has served as a useful guide for mechanistic studies, it is too simplistic to account for such subtle observations as partial or biased agonism.

The structure-function relationships of MCP-1 have been thoroughly examined in a seminal study by Handel and coworkers (*27, 28*). MCP-1 residues T10 (N-terminal region, immediately preceding the CC motif), Y13 and R24 (N-loop), K35 ("30s" loop) and K49 (β3 region) make substantial contributions to CCR2 binding affinity and N-terminal residues I5 and V9 of MCP-1 contribute to signaling via CCR2. Almost all of the MCP-1 residues shown to play key roles in CCR2 binding or activation are identical in MCP-3. Thus, the interactions of these residues are likely to also occur for MCP-3 and do not account for the differences in the CCR2 binding affinity or efficacy of MCP-1 and MCP-3. In good agreement with the previous observations of MCP-1 mutants and the two-site model, our β-arr2 recruitment data for MCP1-311 and MCP3-133 indicate that the chemokine N-terminal region is the major selectivity determinant of receptor activation manifested by changes in the intrinsic efficacy of these different chemokines. However, surprisingly, our analysis of MCP-1/MCP-3 chimeras also identified the N-terminal region as being the primary determinant of the binding selectivity of these two chemokines to CCR2. Residues within this region

were not previously found to contribute to binding affinity, with the sole exception of T10 (*27*), which is identical in MCP-1 and MCP-3. Our results are consistent with the prevailing model that the majority of binding affinity for both chemokines is provided by residues in the N-loop and β3 regions. However, it now appears that these regions contribute equally to the CCR2 binding affinities of both chemokines whereas the N-terminal region of MCP-1 contributes more binding energy compared to the N-terminal region of MCP-3, resulting in the higher binding affinity of MCP-1. In the two-site model, the chemokine N-terminal region corresponds to CS2, which is considered to be the key determinant of receptor activation but not to play a role in the initial binding step. Our results suggest an extension of the two-site model such that CS2/RS2 interactions contribute either to the initial binding step or to the formation of a more stable complex subsequent to initial binding but prior to (or concomitant with) receptor activation.

To identify receptor residues that interact with the N-terminal regions of MCP-1 and/or MCP-3, we mutated residues in CCR2 whose side chains are predicted to point towards the interior of the transmembrane helical bundle. Several of the mutants displayed altered chemokine binding. In particular, mutation of R206$^{5.42}$ or Y259$^{6.51}$ (superscripts indicate Ballesteros-Weinstein numbering (*33*)) completely abolished the ~10-fold binding selectivity of CCR2 for MCP-1 over MCP-3. These residues form a closely packed cluster with residues Y120$^{3.32}$, I263$^{6.55}$ and E291$^{7.39}$ in a region where TM helices 3, 5, 6 and 7 come together, previously defined as the "major subpocket" of the receptor (Fig. 5, A to C) (*34*). In support of the contribution of this structural region to binding, mutation of I263 (in the I263A$^{6.55}$/N266A$^{6.58}$ double mutant) slightly reduced affinity for MCP-3 and mutation of E291$^{7.39}$ slightly reduced affinity for both MCP-1 and MCP-3 (Table 3). Although we cannot exclude the possibility that this cluster of amino acids influences chemokine binding via an indirect, allosteric mechanism, these residues are adjacent to the extreme N-terminus of the bound chemokine in our homology model (Fig. 5, A to C), suggesting that they interact directly with the chemokine ligands. This conclusion is supported by a recent exhaustive mutagenesis study of CXCR4 defining a similar

cluster of signal “initiation residues” adjacent to the N-terminus of CXCL12 (*35*). Notably, in the complex of vMIP-II with CXCR4 from which our homology model was derived, the N-terminus of vMIP-II points slightly away from these residues into the “minor subpocket” of CXCR4 (Fig. 5, D and E) (*21*). Our data suggest that the interactions of the CCR2 major subpocket with the chemokine N-terminus play a critical role in stabilizing the chemokine-receptor complex and in determining the relative affinities of MCP-1 and MCP-3 at their shared receptor.

Among the CCR2 mutations that reduced chemokine binding affinity, the Y259F and I263A/N266A mutations surprisingly caused *increased* potency of MCP-1 and/or MCP-3. This lack of correlation between potency and affinity can be rationalized by considering the possible interactions of these residues in the chemokine-receptor complex prior to undergoing the conformational change required for activation (the inactive state) and after this conformational change (the active state). Our affinity measurements were performed in the presence of guanine nucleotides and therefore are likely to probe interactions in the (G protein-uncoupled) inactive state whereas the potency of ERK1/2 phosphorylation is likely to be more sensitive to interactions in the active state. We suggest that the Y259F and I263A/N266A mutations disrupt interactions in the inactive state but favor the transition to the active state, thereby enhancing potency. In contrast, the R206A and E291A mutants displayed decreased affinity and decreased efficacy of ERK1/2 phosphorylation without any significant change in potency. Disruption of these residues may alter the structure of the active state such that it is no longer well coupled to ERK signaling effectors.

Several CCR2 mutations influenced ERK1/2 phosphorylation without affecting chemokine binding affinity. In particular, the D284A$^{7.32}$ mutation enhanced the potency of ERK phosphorylation in response to MCP-1 and the K34A$^{1.28}$ mutation enhanced the efficacy of ERK phosphorylation in response to both chemokines. These two residues are located adjacent to each other and form a salt bridge in our homology model (Fig. 5B). We propose that these residues do not contribute directly to ligand interactions but instead stabilize the inactive state of the receptor by interacting

with each other and/or with other residues on adjacent TM helices. Disruption of these interactions may therefore facilitate the transition to the active state, albeit at the expense of destabilizing the unbound receptor structure.

Conclusion

We have shown that the distinct affinities and efficacies of CCR2 activation by MCP chemokines can be primarily attributed to the interactions of the chemokine N-terminal region, suggesting an elaboration of the two-site model in which the chemokine N-terminus contributes to binding interactions prior to receptor activation. By analysis of CCR2 mutants, we have identified a cluster of CCR2 residues nestled between transmembrane helices 3, 5, 6 and 7 that appears to be the key binding site for the chemokine N-terminus. Considering that the equivalent residues of chemokine receptor CCR5 comprise a substantial part of the binding site for the anti-HIV drug maraviroc (Fig. 5, F and G) (*36*), our results suggest that this site within CCR2 may also be a suitable target for future development of small molecule inhibitors with potential applications in atherosclerosis, obesity/diabetes and other macrophage-associated inflammatory diseases.

Materials and Methods

Details are provided in the Supplementary Material.

Wild type and chimeric chemokines

Chimeras of human chemokines MCP-1 (obligate monomeric mutant P8A) and MCP-3 (Fig. 2) consisted of the sequence of one chemokine with one or more of the following three regions replaced by the corresponding residues from the other chemokine: N-terminus (residues 1-10); N-loop (residues 12-24); β3 region (residues 46-52). For N-loop substitutions, residue V22 (MCP-1) or K22 (MCP-3) was not replaced and, for β3 region substitutions, residue I46 (MCP-1) or K46 (MCP-3) was not replaced because these residues are buried in the hydrophobic core and mutation would be expected to disrupt the protein fold. Genes encoding the chimeras were constructed by recursive PCR and ligated into pET28a plasmid for expression. Amino acid sequences of the chemokines and chimeras are listed in fig. S7. All chemokines and chimeras were expressed and purified as described by Tan *et al* (*37*). Protein identity was confirmed by MALDI-TOF mass spectrometry (Table S3). ^{1}H NMR spectra were recorded at 25 °C and 600 MHz.

CCR2 mutants

A homology model of human CCR2 bound to human MCP-1 was constructed based on the crystal structure of CXCR4 bound (and cross-linked) to the viral chemokine vMIP-II (PDB code: 4RWS) (*21*). Individual CCR2 residues or pairs of residues were selected for mutation based on their locations and orientations in the predicted chemokine binding site on the interior of the TM helical bundle. The wild type and mutant c-Myc-FLAG-CCR2 constructs in pcDNA5/FRT/TO (*37*) were stably transfected into HEK293 Flp-In TRex cells for all use in all cell-based assays. CCR2 expression was measured using anti-c-Myc ELISA as described (*38*).

CCR2 binding and activation assays

Competitive binding assays were performed as described by Zweemer *et al*. (*39*) using membranes prepared from the CCR2-expressing cells. Recruitment of β-arrestin-2 to CCR2 was assessed in HEK293 Flp-In TRex transiently transfected with CCR2-RLuc8 and β-arrestin-2-YFP as described (*40*). Phosphorylation of ERK1/2 in c-Myc-FLAG-CCR2 HEK293 FlpIn TRex cells was measured using the AlphaScreen® SureFire® p-ERK 1/2 (Thr202/Tyr204) Assay Kit (PerkinElmer, TGR biosciences). The ability of ligands to inhibit forskolin-induced cAMP production was assessed in c-Myc-FLAG-CCR2 HEK293 FlpIn TRex cells transiently transfected to express the CAMYEL cAMP BRET biosensor (*38*).

Data analysis and statistics

All data points represent the mean and error bars represent the standard error of the mean (SEM) of at least three independent experiments. All data from concentration-response curves were normalized and fitted and statistics were determined using Prism 6.0 (GraphPad Software Inc., San Diego, CA). All parameters were estimated as logarithms. Multiple T test comparison with Holm-Sidak correction or one way ANOVA were used as stated in Figure Legends. Significance is defined as * for $p< 0.05$, ** for $p<0.01$ and *** for $p < 0.001$ for the comparison graphs.

Supplementary Materials

Detailed Materials and Methods

Fig. S1. Biased agonism for wild type chemokines

Fig. S2. NMR spectra of chemokine chimeras

Fig. S3. Biased agonism of chemokine chimeras

Fig. S4. Positions of CCR2 mutations on homology model

Fig. S5. Concentration response curves for CCR2 mutants

Fig. S6. Graphical comparisons of chemokine binding and activation parameters for CCR2 mutants

Fig. S7. Amino acid sequences of chemokine chimeras

Table S1. Biased agonism analysis for wild type chemokines

Table S2. Biased agonism analysis for chemokine chimeras

Table S3. Mass spectral data for chemokine chimeras

References

1. T. Kenakin, A. Christopoulos, Signalling bias in new drug discovery: detection, quantification and therapeutic impact. *Nat. Rev. Drug Discov.* **12**, 205-216 (2013).
2. T. Kenakin, Functional selectivity and biased receptor signaling. *J. Pharmacol. Exp. Ther.* **336**, 296-302 (2011).
3. W. Huang, A. Manglik, A. J. Venkatakrishnan, T. Laeremans, E. N. Feinberg, A. L. Sanborn, H. E. Kato, K. E. Livingston, T. S. Thorsen, R. C. Kling, S. Granier, P. Gmeiner, S. M. Husbands, J. R. Traynor, W. I. Weis, J. Steyaert, R. O. Dror, B. K. Kobilka, Structural insights into micro-opioid receptor activation. *Nature* **524**, 315-321 (2015).
4. A. Manglik, T. H. Kim, M. Masureel, C. Altenbach, Z. Yang, D. Hilger, M. T. Lerch, T. S. Kobilka, F. S. Thian, W. L. Hubbell, R. S. Prosser, B. K. Kobilka, Structural Insights into the Dynamic Process of β2-Adrenergic Receptor Signaling. *Cell* **161**, 1101-1111 (2015).
5. S. G. Rasmussen, B. T. DeVree, Y. Zou, A. C. Kruse, K. Y. Chung, T. S. Kobilka, F. S. Thian, P. S. Chae, E. Pardon, D. Calinski, J. M. Mathiesen, S. T. Shah, J. A. Lyons, M. Caffrey, S. H. Gellman, J. Steyaert, G. Skiniotis, W. I. Weis, R. K. Sunahara, B. K. Kobilka, Crystal structure of the beta2 adrenergic receptor-Gs protein complex. *Nature* **477**, 549-555 (2011).
6. B. Moser, M. Wolf, A. Walz, P. Loetscher, Chemokines: multiple levels of leukocyte migration control. *Trends Immunol.* **25**, 75-84 (2004).
7. M. Baggiolini, Chemokines in pathology and medicine. *J. Intern. Med.* **250**, 91-104 (2001).

8. C. Gerard, B. J. Rollins, Chemokines and disease. *Nat. Immunol.* **2**, 108-115 (2001).

9. A. E. Proudfoot, Chemokine receptors: multifaceted therapeutic targets. *Nat. Rev. Immunol.* **2**, 106-115 (2002).

10. R. Martinelli, I. Sabroe, G. LaRosa, T. J. Williams, J. E. Pease, The CC chemokine eotaxin (CCL11) is a partial agonist of CC chemokine receptor 2B. *J. Biol. Chem.* **276**, 42957-42964 (2001).

11. A. Mueller, N. G. Mahmoud, M. C. Goedecke, J. A. McKeating, P. G. Strange, Pharmacological characterization of the chemokine receptor, CCR5. *Brit. J. Pharmacol.* **135**, 1033-1043 (2002).

12. Y. Wan, J. P. Jakway, H. Qiu, H. Shah, C. G. Garlisi, F. Tian, P. Ting, D. Hesk, R. W. Egan, M. M. Billah, S. P. Umland, Identification of full, partial and inverse CC chemokine receptor 3 agonists using [35S]GTPgammaS binding. *Eur. J. Pharmacol. (Mol. Pharmacol. Sect.)* **456**, 1-10 (2002).

13. Y. A. Berchiche, S. Gravel, M. E. Pelletier, G. St-Onge, N. Heveker, Different effects of the different natural CC chemokine receptor 2b ligands on beta-arrestin recruitment, Galphai signaling, and receptor internalization. *Mol. Pharmacol.* **79**, 488-498 (2011).

14. C. T. Veldkamp, C. Seibert, F. C. Peterson, N. B. De la Cruz, J. C. Haugner, 3rd, H. Basnet, T. P. Sakmar, B. F. Volkman, Structural basis of CXCR4 sulfotyrosine recognition by the chemokine SDF-1/CXCL12. *Sci. Signal.* **1**, ra4 (2008).

15. S. Rajagopal, S. Ahn, D. H. Rominger, W. Gowen-MacDonald, C. M. Lam, S. M. Dewire, J. D. Violin, R. J. Lefkowitz, Quantifying ligand bias at seven-transmembrane receptors. *Mol. Pharmacol.* **80**, 367-377 (2011).

16. J. Corbisier, C. Gales, A. Huszagh, M. Parmentier, J. Y. Springael, Biased signaling at chemokine receptors. *J. Biol. Chem.* **290**, 9542-9554 (2015).

17. S. Colin, G. Chinetti-Gbaguidi, B. Staels, Macrophage phenotypes in atherosclerosis. *Immunol. Rev.* **262**, 153-166 (2014).

18. Y. Bai, Q. Sun, Macrophage recruitment in obese adipose tissue. *Obesity Rev.* **16**, 127-136 (2015).

19. S. Struyf, E. Van Collie, L. Paemen, W. Put, J. P. Lenaerts, P. Proost, G. Opdenakker, J. Van Damme, Synergistic induction of MCP-1 and -2 by IL-1beta and interferons in fibroblasts and epithelial cells. *J. Leukocyte Biol.* **63**, 364-372 (1998).

20. B. Qiu, K. A. Frait, F. Reich, E. Komuniecki, S. W. Chensue, Chemokine expression dynamics in mycobacterial (type-1) and schistosomal (type-2) antigen-elicited pulmonary granuloma formation. *Am. J. Pathol.* **158**, 1503-1515 (2001).

21. L. Qin, I. Kufareva, L. G. Holden, C. Wang, Y. Zheng, C. Zhao, G. Fenalti, H. Wu, G. W. Han, V. Cherezov, R. Abagyan, R. C. Stevens, T. M. Handel, Structural biology. Crystal structure of the chemokine receptor CXCR4 in complex with a viral chemokine. *Science* **347**, 1117-1122 (2015).

22. J. S. Burg, J. R. Ingram, A. J. Venkatakrishnan, K. M. Jude, A. Dukkipati, E. N. Feinberg, A. Angelini, D. Waghray, R. O. Dror, H. L. Ploegh, K. C. Garcia, Structural biology. Structural basis for chemokine recognition and activation of a viral G protein-coupled receptor. *Science* **347**, 1113-1117 (2015).

23. J. W. Black, P. Leff, N. P. Shankley, J. Wood, An operational model of pharmacological agonism: the effect of E/[A] curve shape on agonist dissociation constant estimation. *Brit. J. Pharmacol.* **84**, 561-571 (1985).

24. T. Kenakin, C. Watson, V. Muniz-Medina, A. Christopoulos, S. Novick, A simple method for quantifying functional selectivity and agonist bias. *ACS Chem. Neurosci.* **3**, 193-203 (2012).

25. T. Kenakin, Quantifying biological activity in chemical terms: a pharmacology primer to describe drug effect. *ACS Chem. Biol.* **4**, 249-260 (2009).

26. I. Clark-Lewis, B. Dewald, M. Loetscher, B. Moser, M. Baggiolini, Structural requirements for interleukin-8 function identified by design of analogs and CXC chemokine hybrids. *J. Biol. Chem.* **269**, 16075-16081 (1994).

27. S. Hemmerich, C. Paavola, A. Bloom, S. Bhakta, R. Freedman, D. Grunberger, J. Krstenansky, S. Lee, D. McCarley, M. Mulkins, B. Wong, J. Pease, L. Mizoue, T. Mirzadegan, I. Polsky, K. Thompson, T. M. Handel, K. Jarnagin, Identification of residues in the monocyte chemotactic protein-1 that contact the MCP-1 receptor, CCR2. *Biochemistry* **38**, 13013-13025 (1999).

28. K. Jarnagin, D. Grunberger, M. Mulkins, B. Wong, S. Hemmerich, C. Paavola, A. Bloom, S. Bhakta, F. Diehl, R. Freedman, D. McCarley, I. Polsky, A. Ping-Tsou, A. Kosaka, T. M. Handel, Identification of surface residues of the monocyte chemotactic protein 1 that affect signaling through the receptor CCR2. *Biochemistry* **38**, 16167-16177 (1999).

29. M. P. Crump, J. H. Gong, P. Loetscher, K. Rajarathnam, A. Amara, F. Arenzana-Seisdedos, J. L. Virelizier, M. Baggiolini, B. D. Sykes, I. Clark-Lewis, Solution structure and basis for functional activity of stromal cell-derived factor-1; dissociation of CXCR4 activation from binding and inhibition of HIV-1. *EMBO J.* **16**, 6996-7007 (1997).

30. J. H. Gong, I. Clark-Lewis, Antagonists of monocyte chemoattractant protein 1 identified by modification of functionally critical NH2-terminal residues. *The Journal of experimental medicine* **181**, 631-640 (1995).

31. I. Clark-Lewis, I. Mattioli, J. H. Gong, P. Loetscher, Structure-function relationship between the human chemokine receptor CXCR3 and its ligands. *The Journal of biological chemistry* **278**, 289-295 (2003).

32. A. B. Kleist, A. E. Getschman, J. J. Ziarek, A. M. Nevins, P. A. Gauthier, A. Chevigne, M. Szpakowska, B. F. Volkman, New paradigms in chemokine receptor signal transduction: Moving beyond the two-site model. *Biochem. Pharmacol.* **114**, 53-68 (2016).

33. J. A. Ballesteros, H. Weinstein, in *Methods in Neurosciences,* S. C. Sealfon, Ed. (Academic Press, San Diego, 1995), vol. 25, pp. 366-428.

34. L. Roumen, D. J. Scholten, P. de Kruijf, I. J. de Esch, R. Leurs, C. de Graaf, C(X)CR in silico: Computer-aided prediction of chemokine receptor-ligand interactions. *Drug Discov. Today Technol.* **9**, e281-291 (2012).

35. M. P. Wescott, I. Kufareva, C. Paes, J. R. Goodman, Y. Thaker, B. A. Puffer, E. Berdougo, J. B. Rucker, T. M. Handel, B. J. Doranz, Signal transmission through the CXC chemokine receptor 4 (CXCR4) transmembrane helices. *Proceedings of the National Academy of Sciences of the United States of America* **113**, 9928-9933 (2016).

36. Q. Tan, Y. Zhu, J. Li, Z. Chen, G. W. Han, I. Kufareva, T. Li, L. Ma, G. Fenalti, W. Zhang, X. Xie, H. Yang, H. Jiang, V. Cherezov, H. Liu, R. C. Stevens, Q. Zhao, B. Wu, Structure of the CCR5 chemokine receptor-HIV entry inhibitor maraviroc complex. *Science* **341**, 1387-1390 (2013).

37. J. H. Y. Tan, M. Canals, J. P. Ludeman, J. Wedderburn, C. Boston, S. J. Butler, A. M. Carrick, T. R. Parody, D. Taleski, A. Christopoulos, R. J. Payne, M. J. Stone, Design and Receptor Interactions of Obligate Dimeric Mutant of Chemokine Monocyte Chemoattractant Protein-1 (MCP-1). *J. Biol. Chem.* **287**, 14692-14702 (2012).

38. D. J. Scholten, M. Canals, M. Wijtmans, S. de Munnik, P. Nguyen, D. Verzijl, I. J. de Esch, H. F. Vischer, M. J. Smit, R. Leurs, Pharmacological characterization of a small-molecule agonist for the chemokine receptor CXCR3. *Brit. J. Pharmacol.* **166**, 898-911 (2012).

39. A. J. Zweemer, I. Nederpelt, H. Vrieling, S. Hafith, M. L. Doornbos, H. de Vries, J. Abt, R. Gross, D. Stamos, J. Saunders, M. J. Smit, A. P. Ijzerman, L. H. Heitman, Multiple binding sites for small-molecule antagonists at the CC chemokine receptor 2. *Mol. Pharmacol.* **84**, 551-561 (2013).

40. M. A. Ayoub, Y. Zhang, R. S. Kelly, H. B. See, E. K. M. Johnstone, E. A. McCall, J. H. Williams, D. J. Kelly, K. D. G. Pfleger, Functional Interaction between Angiotensin II Receptor Type 1 and

Chemokine (C-C Motif) Receptor 2 with Implications for Chronic Kidney Disease. *Plos One* **10**, (2015).

Acknowledgments: We thank Dr. Holly Yeatman and Justin Ludeman for technical assistance. **Funding**: Supported by Australian Research Council Discovery Grant DP120100194 and LIEF Grant LE0989504 (M.J.S.), Monash Institute of Pharmaceutical Sciences Large Grant Support Scheme (M.C.) and ANZ Trustees Grant 12-3831 (M.J.S. and M.C.). K.D.G.P. is a NHMRC RD Wright Career Development Fellow (1085842), J.R.L. is a Monash University Larkins Fellow and an RD Wright Career Development Fellow. M.C. is a Monash Fellow. **Author contributions**: Z.H. and J.S. participated in research design and performed experiments; H.L. performed and supervised radioligand binding assays; J.B. generated preliminary data; C.H. performed and interpreted mass spectrometry; B.J.P. and B.T.P. generated homology models. J.G.P. contributed to chimera design and preparation. K.D.G.P. provided the CCR2-RLuc8 construct for BRET assays. J.R.L., M.C. and M.J.S. interpreted the results and wrote the manuscript. M.C. and M.J.S. conceived the studies and designed the experiments. All authors read and critically reviewed the manuscript. **Competing interests:** N/A**. Data and materials availability:** N/A

	β-arrestin recruitment		cAMP inhibition		ERK 1/2 phosphorylation		^{125}I-MCP1 binding
	pEC_{50}	E_{max}	pEC_{50}	E_{max}	pEC_{50}	E_{max}	pK_i
MCP-1	8.32 ± 0.06	100 ± 2	9.10 ± 0.21	100 ± 9	9.16 ± 0.24	100 ± 10	10.60 ± 0.08
MCP-2	7.24 ± 0.26 *	23 ± 3 ***	7.34 ± 0.14 ***	113 ± 9	7.58 ± 0.15 ***	119 ± 9	8.88 ± 0.14 ***
MCP-3	7.33 ± 0.15 *	56 ± 4 **	8.47 ± 0.16 *	109 ± 9	8.09 ± 0.19 ***	116 ± 10	9.50 ± 0.12 ***

Table 1: Potency, efficacy and affinity of the different MCP chemokines at the hCCR2 receptor in β-arrestin recruitment, Fsk-induced cAMP inhibition, pERK and radioligand binding assays. β-arrestin 2 recruitment was assessed using BRET in FlpInTRex 293 cells transiently transfected with CCR2-RLuc8 and β-arr2-YFP. Inhibition of cAMP was measured using a BRET-based cAMP sensor transiently transfected in c-Myc-FLAG-hCCR2 FlpInTRex 293 cells. ERK1/2 phosphorylation was measured 3 min after chemokine stimulation in c-Myc-FLAG-hCCR2 FlpInTRex 293 cells. ^{125}I-MCP-1 competition binding was measured in membrane preparations of c-Myc-FLAG-hCCR2 FlpInTRex 293 cells. pEC_{50} and pK_i values are the negative log of EC_{50} and K_i values, respectively, in molar units. E_{max} values are reported as a percentage of the value for MCP-1. Data are mean ± SEM from 3-4 experiments performed in triplicate. * P<0.05, ** P<0.01, *** P<0.001, one-way ANOVA with Dunnett's multiple comparison test. E_{max} is shown relative to that observed with MCP-1.

	β-arrestin recruitment		ERK 1/2 phosphorylation		^{125}I-MCP1 binding
	pEC_{50}	E_{max}	pEC_{50}	E_{max}	pK_i
MCP-1	8.00 ± 0.13	0.100 ± 0.006^^^	7.87 ± 0.32	37.8 ± 3.4	10.67 ± 0.18 ^^
MCP1-311	7.30 ± 0.21	0.067 ± 0.006*	6.84 ± 0.17	40.3 ± 3.2	9.90 ± 0.18
MCP1-131	8.32 ± 0.13	0.11 2± 0.006^^^	7.64 ± 0.26	43.7 ± 3.7	10.53 ± 0.17 ^^
MCP1-113	8.12 ± 0.13	0.111 ± 0.006^^^	7.58 ± 0.46	46.7 ± 6.8	10.68 ± 0.16 ^^
MCP1-133	8.45 ± 0.27	0.103 ± 0.009^^	7.86 ± 0.42	36.4 ± 5.0	10.84 ± 0.16 ^^
MCP1-333	7.82 ± 0.58	0.034 ± 0.009***	6.95 ± 0.29	24.0 ± 3.1	10.02 ± 0.17
MCP-3	7.63 ± 0.17	0.060 ± 0.004**	7.21 ± 0.31	34.3 ± 4.0	9.50 ± 0.19 **
MCP3-133	8.24 ± 0.11	0.0135 ± 0.005^^^	8.12 ± 0.33	25.9 ± 2.3	10.36 ± 0.14
MCP3-313	7.17 ± 0.22	0.051 ± 0.006***	7.43 ± 0.27	33.1 ± 3.0	7.45 ± 0.23 ***, ^^
MCP3-331	7.65 ± 0.22	0.056 ± 0.006**	7.66 ± 0.36	21.7 ± 2.3*	8.77 ± 0.33 ***
MCP3-311	7.13 ± 0.39	0.050 ± 0.010***	7.87 ± 0.14	40.0 ± 1.6	7.32 ± 0.32 ***, ^^
MCP3-111	7.61 ± 0.20	0.134 ± 0.010^^^	7.99 ± 0.36	21.3 ± 2.4*	9.80 ± 0.17

Table 2: Potency, efficacy and affinity of the MCP chemokine chimeras at the hCCR2 receptor in β-arrestin recruitment, pERK and radioligand binding assays. ^{125}I-MCP-1 competition binding was measured in membrane preparations of c-Myc-FLAG-hCCR2 FlpInTRex 293 cells. β-arrestin 2 recruitment was assessed using BRET in FlpInTRex 293 cells transiently transfected with CCR2-RLuc8 and β-arr2-YFP. ERK1/2 phosphorylation was measured 3-5 min after chemokine stimulation in c-Myc-FLAG-hCCR2 FlpInTRex 293 cells. pEC_{50} and pK_i values are the negative log of EC_{50} and K_i values, respectively, in molar units. E_{max} values are relative to the positive control. Data are mean ± SEM from 3-4 experiments performed in triplicate. * P<0.05, **,^^ P<0.01, ***,^^^ P<0.001, compared to MCP-1 or MCP-3 respectively; one-way ANOVA with Dunnett's multiple comparison text.

Mutation	Location[#]	Cell surface expression	pK_i		pERK1/2 pEC_{50}		pERK1/2 E_{max} (% FBS)	
			MCP-1	MCP-3	MCP-1	MCP-3	MCP-1	MCP-3
WT		100 ± 3	10.82 ± 0.18	9.64 ± 0.19^	8.01 ± 0.23	7.30 ± 0.23	38.9 ± 3	35.5 ± 4.5
K34A	TM1 (1.28)	119 ± 12	10.42 ± 0.27	9.70 ± 0.42	8.41 ± 0.24	7.70 ± 0.23	55.5 ± 2.5***	45.0 ± 2.8
Y120F	TM3 (3.32)	118 ± 13	11.15 ± 0.18	9.65 ± 0.26^	7.92 ± 0.32	7.58 ± 0.33	25.4 ± 2**	16.6 ± 1.6***
V187/V189A	ECL2	108 ± 6	11.36 ± 0.29	9.85 ± 0.32^	7.99 ± 0.26	7.28 ± 0.23	30.5 ± 2	30.8 ±2.3
N199A/T203A	TM5 (5.35/5.39)	116 ± 7	11.42 ± 0.29	10.17 ± 0.47	7.66 ± 0.23	7.35 ± 0.33	32.8 ± 2	20.2 ± 2.3**
R206A	TM5 (5.42)	112 ± 7	10.29 ± 0.22	10.12 ± 0.33	8.25 ± 0.31	7.81 ± 0.34	11.0 ± 0.8***	14.8 ± 2.5***
Y259F	TM6 (6.51)	99 ± 6	10.44 ± 0.23	10.20 ± 0.14	8.78 ± 0.36*	8.57 ± 0.26**	31.9 ± 1.7	39.3 ± 1.7
I263A/N266A	TM6 (6.55/6.58)	107 ± 8	10.79 ± 0.24	8.99 ± 0.17^	9.46 ± 0.39**	8.22 ± 0.38	24.7 ± 2***	36.9 ± 3.4
E270A/F272A	TM6/ECL3	99 ± 13	11.68 ± 0.39	10.06 ± 0.31^	7.36 ± 0.20	7.36 ± 0.20	22.3 ± 1.3***	22.1 ± 1.5**
D284A	TM7 (7.32)	104 ± 5	10.91 ± 0.16	9.52 ± 0.25^	8.83 ± 0.40**	7.80 ± 0.18	34.9 ± 2	39.1 ± 1.9
E291A	TM7 (7.39)	107 ± 9	10.26 ± 0.24	9.03 ± 0.22^	7.66 ± 0.40	7.09 ± 0.48	27.9 ± 3*	12.1 ± 2.2***

Table 3: Characterization of CCR2 mutants. Cell surface expression was measured by anti c-Myc ELISA in c-Myc-FLAG-hCCR2 FlpInTRex 293 cells (expressed as a percentage of WT receptor). Affinity (pK_i) of MCP-1 and MCP-3 for WT or mutant CCR2 was measured by ^{125}I-MCP-1 competition binding with cell membrane preparations. Potency (pEC_{50}) and efficacy (E_{max}) of MCP-1 and MCP-3 for WT or mutant CCR2 in ERK1/2 phosphorylation was measured 3 min after chemokine stimulation in c-Myc-FLAG-hCCR2 FlpInTRex 293 cells. pEC_{50} and pK_i values are the negative log of EC_{50} and K_i values, respectively, in molar units. E_{max} values are relative to the positive control. Data are mean ± SEM from 3-4 experiments performed in triplicate. For radioligand binding, ^ P<0.05, compared to MCP-1 for each mutant, multiple t-test. For ERK1/2 phosphorylation, * P<0.05, ** P<0.01, *** P<0.001,

compared to CCR2 WT, one-way ANOVA with Dunnett's multiple comparison test. [#] Ballesteros and Weinstein numbering of TM residues shown in parentheses (*33*).

Figure Legends

Figure 1. MCP chemokines display different efficacies and affinities at the hCCR2. (A) β-arrestin 2 recruitment was assessed using BRET in FlpInTRex 293 cells transiently transfected with CCR2-RLuc8 and β-arr2-YFP. **(B)** Inhibition of cAMP was measured using a BRET-based cAMP sensor transiently transfected in c-Myc-FLAG-hCCR2 FlpInTRex 293 cells. **(C)** ERK1/2 phosphorylation was measured 3 min after chemokine stimulation in c-Myc-FLAG-hCCR2 FlpInTRex 293 cells. **(D)** ^{125}I-MCP-1 competition binding was measured in membrane preparations of c-Myc-FLAG-hCCR2 FlpInTRex 293 cells. **(E)** Time-course of receptor internalization in response to 100 nM of MCPs detected in c-Myc-FLAG-hCCR2 FlpInTRex 293 cells by whole cell anti c-Myc ELISA. Data are means ± SEM from 3-5 experiments performed in triplicate. * P<0.05, ** P<0.01, *** P<0.001, **** P<0.0001 one-way ANOVA with Dunnett's multiple comparison test.

Figure 2. Design and structural validation of MCP-1/MCP-3 chimeras. (A) Aligned sequences of MCP-1 and MCP-3 with the three regions swapped in the chimeras indicated by boxes. Symbols above the residue labels indicate those previously found to be important in CCR2 binding (*) or activation (^) (*27, 28*). **(B)** The structure of MCP-1 (pdb code: 1dok) highlighting the regions swapped in the chimeras. **(C)** Nomenclature and schematic diagrams of the chimeras with regions from MCP-1 and MCP-3 in blue and red, respectively. **(D)** Upfield (methyl) region of the ^{1}H NMR spectra of WT and chimeric chemokines, showing well-dispersed peaks indicative of correct folding.

Figure 3. The N-terminal tail of MCP-1 and MCP-3 is a major determinant of affinity and efficacy. ^{125}I-MCP-1 competition binding, β-arrestin 2 recruitment BRET and ERK1/2 phosphorylation were assessed for MCP-1 and MCP-3 chimeric chemokines (top/blue and bottom/red, respectively). **(A)** ^{125}I-MCP-1 competition binding was measured in membrane preparations of c-Myc-FLAG-hCCR2 FlpInTRex 293 cells. **(B)** β-arrestin 2 recruitment was assessed using BRET in FlpInTRex 293 cells transiently transfected with CCR2-RLuc8 and β-arr2-YFP. **(C)** ERK1/2 phosphorylation was measured

3 min after chemokine stimulation in c-Myc-FLAG-hCCR2 FlpInTRex 293 cells. **(D)** CCR2 internalization upon stimulation with Vehicle, 100 nM MCP-1, MCP1-311, MCP-3 or MCP3-133 for 60 min was measured in c-Myc-FLAG-hCCR2 FlpInTRex 293 cells by whole cell anti c-Myc ELISA. Data are means ± SEM from 3-5 experiments performed in triplicate. * P<0.05, ** P<0.01, one-way ANOVA with Dunnett's multiple comparison text. **(E)** Affinity (pK_i), potency (pEC_{50}) and efficacy (E_{max}) for WT and chimeric chemokines in ^{125}I-MCP-1 competition binding, β-arrestin 2 recruitment BRET and ERK1/2 phosphorylation. Data are means ± SEM from 3-5 experiments performed in triplicate. * P<0.05, **,^^ P<0.01, ***,^^^ P<0.001, ****,^^^^ P<0.0001 compared to MCP-1 or MCP-3 respectively; one-way ANOVA with Dunnett's multiple comparison text.

Figure 4. Identification of CCR2 residues contributing to MCP-1 and MCP-3 binding and agonism. ^{125}I-MCP-1 competition binding and ERK1/2 phosphorylation were assessed for MCP-1 and MCP-3 at the wild type (WT) and mutant CCR2 expressed in FlpInTRex 293 cells. **(A)** Affinity (pK_i) of MCP-1 (blue) and MCP-3 (red) for WT or mutant CCR2 measured by ^{125}I-MCP-1 competition binding with cell membrane preparations. Right/grey panel: differences in affinity between MCP-1 and MCP-3 at each mutant. ^ P<0.05, compared to the difference observed at the WT and * P<0.05, compared to zero (i.e. indicating difference between chemokines), multiple t-test. **(B)** Potency (pEC_{50}) of MCP-1 (blue) and MCP-3 (red) for WT or mutant CCR2 in ERK1/2 phosphorylation. Right/grey panel: differences in potency between MCP-1 and MCP-3 at each mutant receptor. * P<0.05, ** P<0.01 compared to the difference observed at the WT one-way ANOVA with Dunnett's multiple comparison test. **(C)** Efficacy (E_{max}) of MCP-1 (blue) and MCP-3 (red) for WT or mutant CCR2 in ERK1/2 phosphorylation. Right/grey panel; ratio of efficacies between MCP-1 and MCP-3 at each mutant. * P<0.05, ** P<0.01, *** P<0.001, **** P<0.0001 compared to ratio observed at the WT, one-way ANOVA with Dunnett's multiple comparison test. Data are means ± SEM from 3-5 experiments performed in triplicate.

Figure 5. The major subpocket of CCR2 recognizes the N-termini of MCP chemokines. (A) Full and **(B)** detailed side views and **(C)** end-on view (from the extracellular perspective) showing the homology model of CCR2 bound to MCP-1. CCR2 transmembrane helices are coloured salmon (TM1), orange (TM2), pale yellow (TM3), pale green (TM4), aquamarine (TM5), light blue (TM6) and violet (TM7); other receptor residues are in grey. Side chain sticks are shown for several residues discussed in the text in darker shades of the same colours as the helices in which they are located. MCP-1 is in teal with the N-terminus in rainbow colours from blue (residue 1) to red (residue 10). In (C) the major (M) and minor (m) subpockets are labelled in red. **(D)** and **(E)** The CXCR4:vMIP-II complex (pdb code: 4rws) displayed as in (B) and (C), respectively. **(F)** and **(G)** The CCR5:maraviroc complex (pdb code: 4mbs) displayed as in (B) and (C), respectively; maraviroc is shown as sticks coloured by element (C, green; N, blue; O, red).

Figure 1

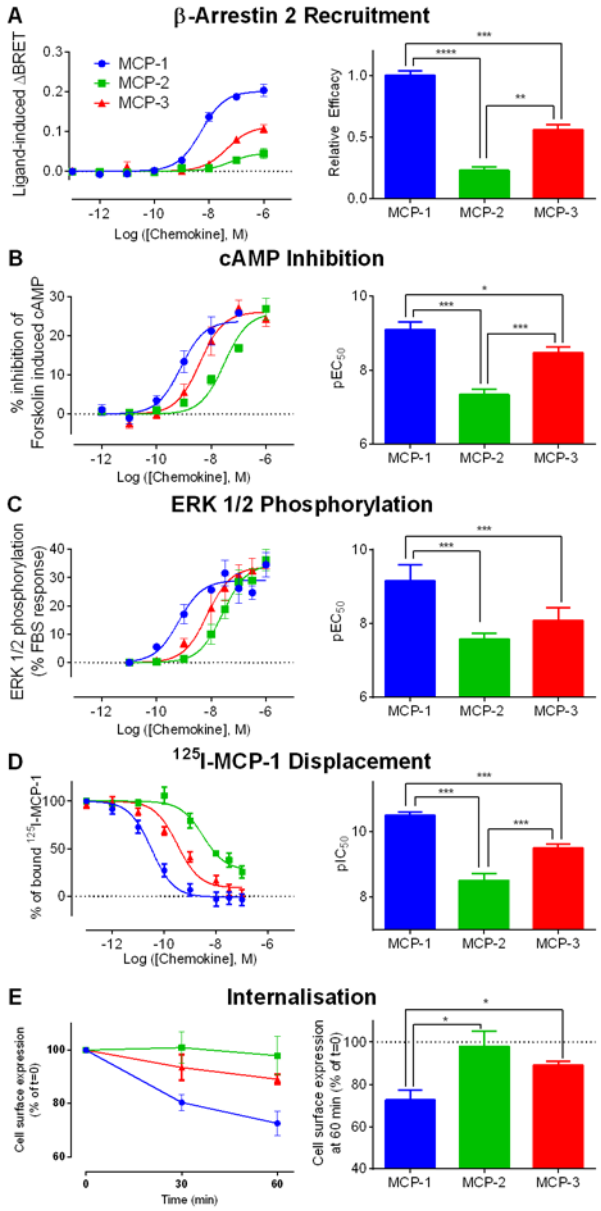
A
β-Arrestin 2 Recruitment
Ligand-induced ΔBRET
MCP-1
MCP-2
MCP-3
Log ([Chemokine], M)
Relative Efficacy
B
cAMP Inhibition
% inhibition of Forskolin induced cAMP
pEC50
C
ERK 1/2 Phosphorylation
ERK 1/2 phosphorylation (% FBS response)
D
125I-MCP-1 Displacement
% of bound 125I-MCP-1
pIC50
E
Internalisation
Cell surface expression (% of t=0)
Time (min)
Cell surface expression at 60 min (% of t=0)

Figure 2

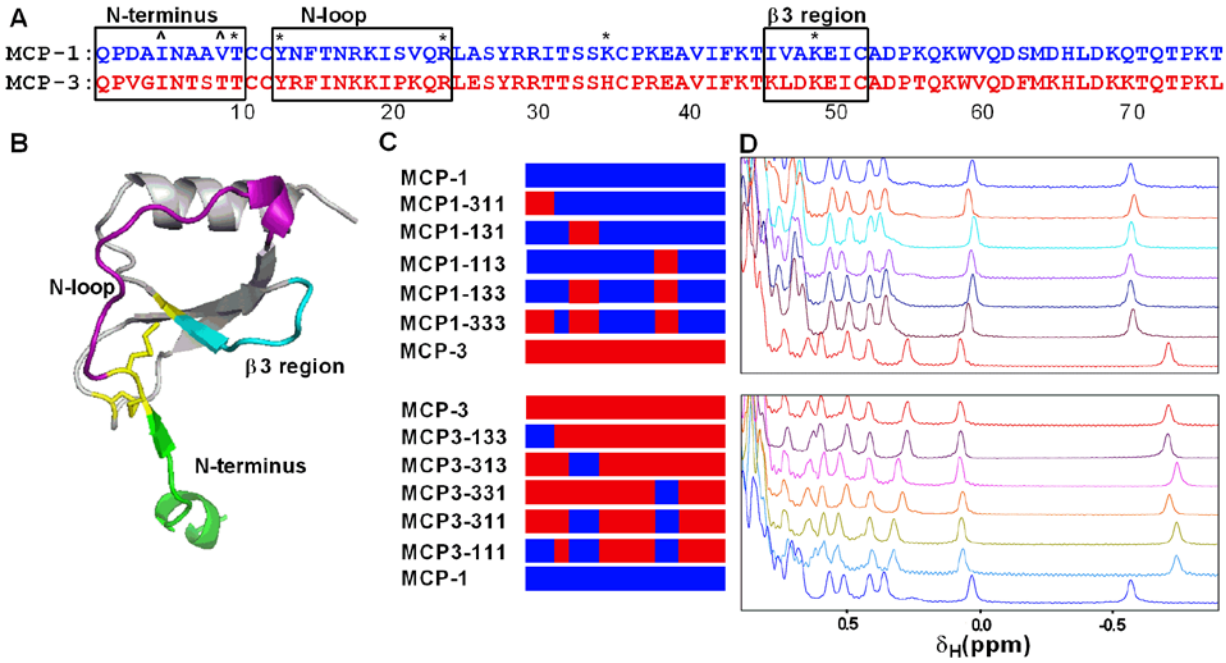
A
N-terminus
N-loop
β3 region
MCP-1 : QPDAINAAVTCCYNFTNRKISVQRLASYRRITSSKCPKEAVIFKTIVAKEICADPKQKWVQDSMDHLDKQTQTPKT
MCP-3 : QPVGINTSTTCCYRFINKKIPKQRLESYRRTTSSHCPREAVIFKTKLDKEICADPTQKWVQDFMKHLDKKTQTPKL
10
20
30
40
50
60
70
B
N-loop
β3 region
N-terminus
C
MCP-1
MCP1-311
MCP1-131
MCP1-113
MCP1-133
MCP1-333
MCP-3
MCP-3
MCP3-133
MCP3-313
MCP3-331
MCP3-311
MCP3-111
MCP-1
D
0.5
0.0
-0.5
δH(ppm)

Figure 3

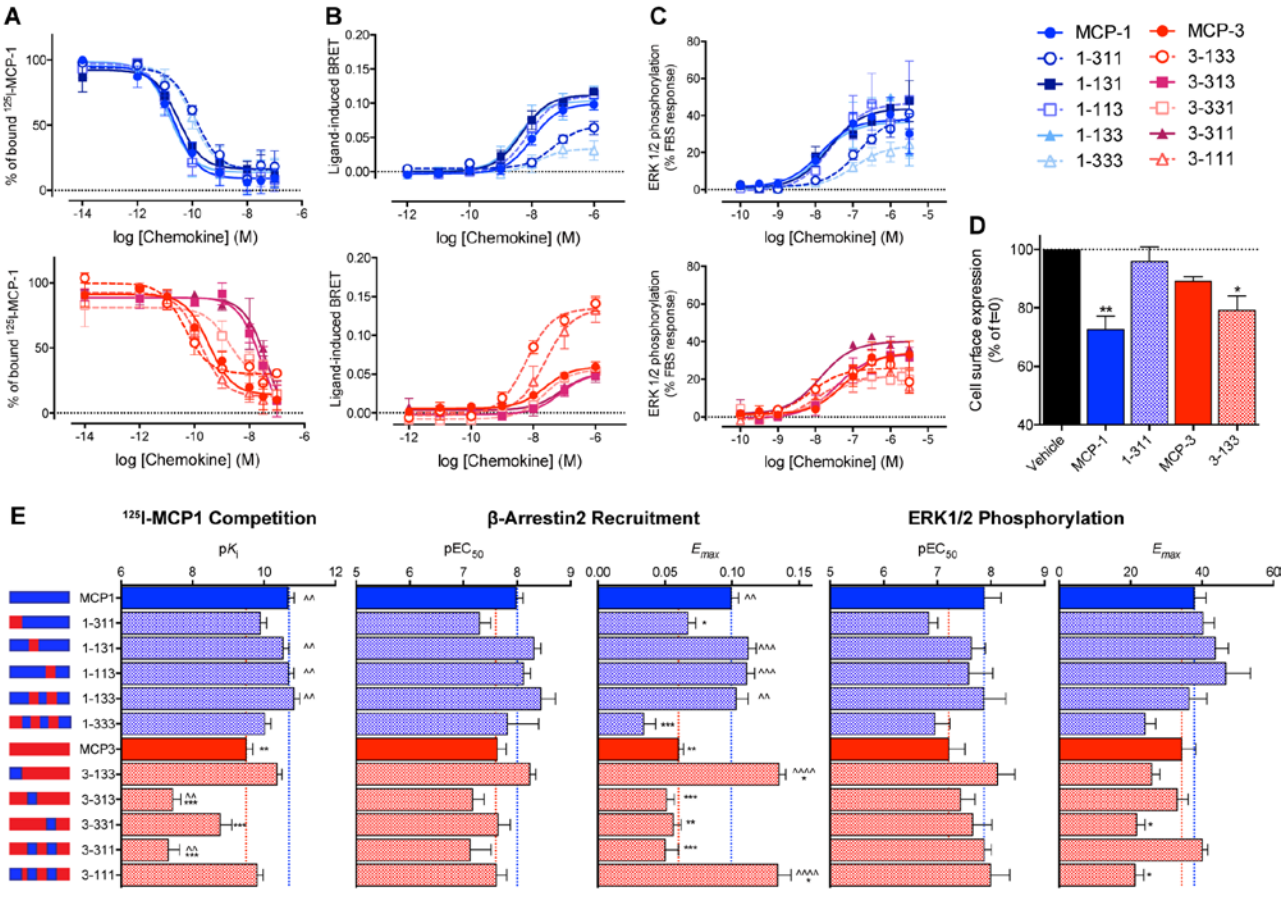
A
B
C
D
E
% of bound 125I-MCP-1
Ligand-induced BRET
ERK 1/2 phosphorylation (% FBS response)
log [Chemokine] (M)
MCP-1
1-311
1-131
1-113
1-133
1-333
MCP-3
3-133
3-313
3-331
3-311
3-111
Cell surface expression (% of t=0)
Vehicle
125I-MCP1 Competition
β-Arrestin2 Recruitment
ERK1/2 Phosphorylation
pKi
pEC50
Emax

Figure 4

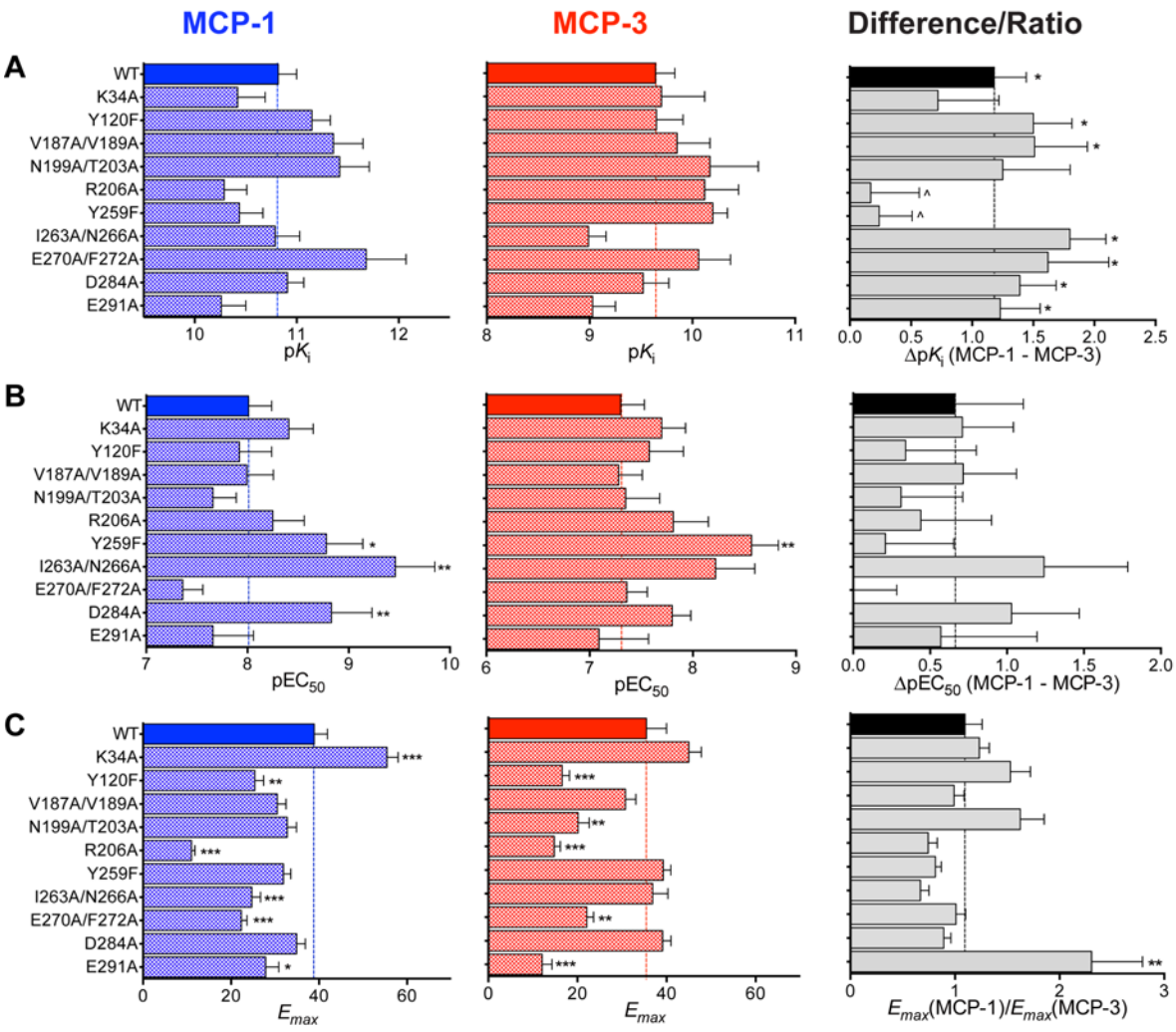
MCP-1
MCP-3
Difference/Ratio
A
WT
K34A
Y120F
V187A/V189A
N199A/T203A
R206A
Y259F
I263A/N266A
E270A/F272A
D284A
E291A
pKi
ΔpKi (MCP-1 - MCP-3)
B
pEC50
ΔpEC50 (MCP-1 - MCP-3)
C
Emax
Emax(MCP-1)/Emax(MCP-3)

Figure 5

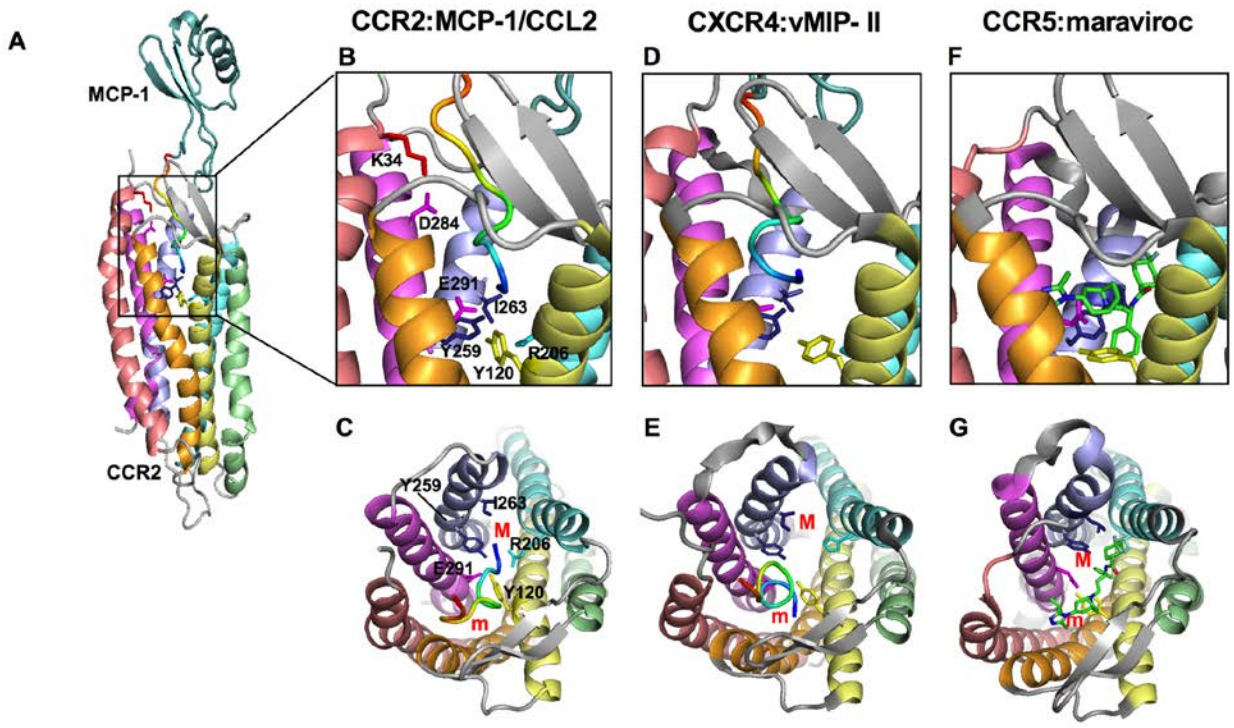
A
MCP-1
CCR2
CCR2:MCP-1/CCL2
CXCR4:vMIP- II
CCR5:maraviroc
B
D
F
K34
D284
E291
I263
Y259
Y120
R206
C
E
G
Y259
I263
M
R206
E291
Y120
m
M
m
M
m